Computational Modeling Framework for the Study of Infectious Disease Spread through Commercial Air-Travel

Pierrot Derjany
Aerospace Engineering Department, Embry Riddle Aeronautical University

Sirish Namilae
Aerospace Engineering Department, Embry Riddle Aeronautical University

Dahai Liu
College of Aviation, Embry Riddle Aeronautical University

Ashok Srinivasan
Department of Computer Science University of West Florida

***Abstract*—This paper presents an integrated computational modelling framework combining pedestrian dynamics and infection spread models, to analyse the infectious disease spread during the different stages of air-travel. While, commercial air travel is central to the global mobility of goods and people, it has also been identified as a leading factor in the spread of several epidemic diseases including influenza, SARS and Ebola. The mixing of susceptible and infectious individuals in these high people density locations like airports involves pedestrian movement which needs to be taken into account in the modelling studies of disease dynamics. We develop a Molecular Dynamics based social force modeling approach for pedestrian dynamics and combine it with a stochastic infection dynamics model to evaluate the spread of viral infectious diseases in airplanes and airports. We apply the multiscale model for various key components of air travel and suggest strategies to reduce the number of contacts and the spread of infectious diseases. We simulate pedestrian movement during boarding and deplaning of some typical commercial airplane models and movement of people through security check areas. We found specific boarding strategies that reduce the number of contacts. Further, we find that smaller airplanes are more effective in reducing the number of contacts compared to larger airplanes. We propose certain queue configuration that reduces contacts between people and mitigate disease spread.**

1. Introduction

Air travel brings together people from different geographic regions with different levels of vulnerability and receptivity due to variations in immunity, ethnic background, and intervention usage across geographic areas [1]. Public transportation in general and air travel in particular have been identified as leading factors in the spread of several infectious diseases including influenza, SARS, tuberculosis, measles and norovirus [2-8]. The high economic and public perception costs on the transportation sector due to epidemic events necessitate transportation policy that addresses mitigation. Our goal is to produce a science-based analysis of public policy options that can lead to mitigating the spread of diseases without disrupting air travel [9-13].

When investigating control strategies to suppress disease propagation among a group or population, the contact pattern between the interacting individuals should be considered and mapped. Contact analysis provides a better insight on the interaction between individuals. We use a new approach in which pedestrian dynamics modeling is used to track the trajectories and evaluate the contacts that could potentially arise among a crowd of infected and susceptible individuals. Pedestrian Dynamics has been addressed using several approaches such as cellular automata [14], fluid flow [15], queuing [16] as well as particle dynamics based approach called social force models [17, 18]. Among these different approaches, social force models have specific advantages for studying passenger movement and contacts in airplanes as each traveller is modelled individually and moves continuously. This enables tracking the individuals' trajectories and estimation of the contacts between pedestrians. Social force models of pedestrian movement are essentially based on molecular dynamics (MD). Social force models extend the concepts of molecular dynamics to pedestrian movement. Here, the forces are a measure of the internal motivation of individual pedestrians to move towards their destination in presence of obstructions like other pedestrians and objects (e.g. walls and chairs).

Social force models have been applied to crowd simulations in panic situations [18], traffic dynamics [19], evacuation [20] and animal herding [21]. Algorithmic developments have included generation of force fields using visual analysis of crowd flows [22], explicit collision prediction[23], and collision avoidance [24]. Here, we apply social force model in a mulitiscale framework to study the pedestrian contact evolution and infectious disease spread during various aspects of air travel.

Movement of pedestrians during air-travel is a special case of a more general problem of pedestrian movement. Several researchers have studied the pedestrian movement at airports especially from the viewpoint of airport operations and reduction of the turnaround time of airplanes at terminals. For instance, Schultz et al. [25] model the intuitive behavior of airport travelers under emergency situation by a cellular automaton model. In this model, the floor area is subdivided into small partitions where pedestrians may switch positions with neighboring spots based on a probabilistic distribution. Several other investigators used agent-based models to model pedestrian motion and passenger flow in airport terminals [26, 27].

Other studies model the flow of pedestrians to their destinations by optimizing the guiding signs [28]. Pedestrian movement in airports is peculiar because it involves a series of nondiscretionary as well as discretionary activities. For example, prior to their scheduled flights, travellers fulfil the trip requirements starting from check-in, security and boarding. Once these processing steps are completed, they are often involved in individual or collective discretionary activities such as dining and shopping at the departure terminal [29, 30]. The airport environment and building layout have a great influence on the passengers' movements, choice and perception of activities preference over a set of alternatives [28, 31]. This uncertainty creates additional challenges in modeling the pedestrian motion at airports. Despite these studies, no work has focused on the effect of pedestrian movement on airborne disease propagation during air travel.

We address this problem through a multiscale model that combines pedestrian dynamics with stochastic infection spread models. The purpose of the pedestrian dynamics model is to generate the trajectories of motion and contacts between infected and susceptible individuals in various travel stages such as enplaning, deplaning and progressing in winding queues for booking or security checking. We incorporate this information into an individual based stochastic infection dynamics model with infection probability and contact radius as primary inputs. Through this multiscale framework, we estimate the aggregate numbers and probabilities of newly infected people during boarding, deplaning and aligning in a security queue. This generic model is applicable for several directly transmitted diseases by varying the input parameters related to infectivity and transmission mechanisms.

2. Modelling Methodology

Pedestrian Dynamics

We model the mobile pedestrians and stationary objects, like walls as particles. The evolution of pedestrian particles and their interaction with other pedestrians and stationary particles are described by a molecular dynamics like social force model [17]. The net force $\bar{f}_i$ acting on *i*th pedestrian (or particle) can be defined as:

$$\bar{f}_i = \frac{m_i}{\tau}\left(\bar{v}_0^i(t) - \bar{v}^i(t)\right) + \sum_{j\neq i}\bar{f}_{ij}(t) = m_i\frac{dv_i}{dt} \qquad (1)$$

with pedestrian position at a given time obtained by numerical integration as $\bar{r}^i(t) = \int \bar{v}^i(t)dt$. $\bar{v}_o^i(t)$ refers to the desired velocity of pedestrian, and $\bar{v}^i(t)$ that of the actual velocity. m_i is the particle's mass and τ is the evolution time constant. The momentum generated by a pedestrian's intention, denoted by $\frac{m_i}{\tau}\left(\bar{v}_0^i(t) - \bar{v}^i(t)\right)$, results in a self-propulsion force that is balanced by a repulsion force $\bar{f}_{ij}(t)$ to obstacles in the direction of motion. In this study we use the Lennard –Jones type repulsion term used earlier by Namilae *et al*. [9, 10].

While equation (1) describes the general motion of pedestrians, we need to introduce modifications to this equation to account for common occurrences observed in crowded locations. One of the common features in places like theme parks, entertainment venues, airport security checkpoints etc., involves formation of slow moving queues. Winding queues are often used to organize waiting crowds in jammed locations, but these results in increased proximate contacts especially if rope separators are used to define the lines. Pedestrians in a queue move at the speed of the nearest person ahead in the line. To model this scenario, we introduce location dependence to the desired velocity in the self-propulsion term as:

$$v_0^i(t)\,\hat{e}_1 = \begin{cases} (v_A + \gamma_i v_B)\left(1 - \frac{\delta}{\min\{r_{ij}|_{front}\,;\, i\neq j\}}\right)\hat{e}_1 \\ 0\,;\, if\ r_{ij}|_{front} < \delta \end{cases} \qquad (2)$$

$$\text{Where } \delta = \begin{cases} \delta_1\,;\, if\ i\ \&\ j\ of\ same\ group \\ \delta_2\,;\, if\ i\ \&\ j\ of\ different\ groups \end{cases}$$

$\hat{e}_1$ is the desired direction of motion. v_A and $\gamma_i v_B$ are the deterministic and stochastic components of the desired velocity respectively. The values of walking speed terms (v_A and $\gamma_i v_B$) can be varied to obtain a given distribution of age groups and gender of travelers [32]. δ is the cut-off distance constant between the *i*th and *j*th pedestrians at which the desired velocity of the *i*th pedestrian reduces to zero velocity (stationary condition).

For accurate simulations that mimic the real life scenario, we also account for the formation of groups of pedestrians. The groups' formation is controlled by adjusting the distance (δ) in equation (2). Our empirical observations on a theme park queue reported elsewhere and comparisons with literature [33], indicate that δ separation values are different between pedestrians belonging to a group (e.g. family or friends in queue) and other pedestrians. Based on this, an average distance of δ_1 =0.46 m (18in) is chosen for pedestrian particles within the same group, while this distance between independent pedestrians is given a value of δ_2 =0.64 m (25 in).

Contact estimation and infection model

Consider a population of size N consisting of I(t) infected and S(t) susceptibles at time t. A susceptible can become infected when coming into direct contact with an infected. Given the trajectory of pedestrians over time, the number of contacts m_i can be evaluated as:

$$m_i(t) = \sum_j r_{ij}.\lambda_{ij}\,, \quad \text{where } \lambda_{ij} = 0 \text{ if } r_{ij} > x \text{ and } \lambda_{ij} = \frac{1}{r_{ij}} \text{ if } r_{ij} < x \qquad (3)$$

Here, r_{ij} is the distance between *i* and *j* pedestrians and *x* is a virus specific distance parameter. Pedestrian position

($r_i(t)$) evolves through pedestrian dynamics and is a function of the age, sex and infection status.

The transmission distance (x) used to define the contact is dependent on the type of pathogen and mechanisms for its spread. For diseases like Ebola, studies indicate that primary mode of transmission is through contact droplets [34-36]. Consequently, a distance that enables direct touch needs to be used for estimating contacts for such diseases. Other infectious diseases like SARS are known to be transmitted by both shorter and longer range airborne mechanisms [37, 38]. Likewise, the influenza can be transmitted through coarse droplets or microscale bioaerosols being respired into the respiratory tract of a susceptible individual [39]. Studies suggest that transmission occurs when the virus particles are suspended in air and inhaled by a susceptible individual or when that individual touches a contaminated surface with deposited droplets and then touches their eyes, nose or mouth [39]. The size of these particles can play an important role in contagion dispersion. Small particles dispersed in aerosols transmit over large distances. For example, experiments indicate micrometer sized aerosol clouds generated during cough traveling over 2 m [40, 41].

Consider that the infection spread initiates due to the insertion of i_c^0 infectives initially (t_0= 0) at their "c" days of infection, out of "d" incubation days. Denote by P_{inf} the probability that a contact between a susceptible and an infective (or contaminated surface) results in infection of the susceptible. We divide this input parameter into two components: a viral shedding probability distribution (P_c) which is a function of time since acquiring infection for specific virus in question, and a pathogen spread mechanism component (P_m). This includes contributions of several independent mechanisms comprising (a) aerosol exposure and inhalation probability (P_a) common in infections such as Norovirus [42] and Ebola [43], (b) Coarse pathogen droplet inoculation (P_d) common in influenza and SARS [7]. Other mechanisms including fomite mechanism, which involves contaminated surface-to-hand transfer would contribute to the infection spread, but such mechanisms do not involve human-to-human contact in this context. The infection probability would then be defined as:

$$P_{\text{inf}} = P_c.P_m = P_c\left(P_a + P_d\right) \qquad (4)$$

Consider the viral shedding probability distribution (P_c). Studies indicate that the amount of viral shedding is typically dependent on the days post symptom appearance for the infected individual and the length of incubation period. In a previous study [9, 10], we used CDC data on amount of RNA (ribonucleic acid) virus copies in the blood serum since the illness contraction to generate this probability distribution for Ebola in Figure 1.a [44]. Similar approach can be used for other diseases, for example, for SARS pathogen (Figure 1.b), the viral gene expression of the nucleocapsid (N) protein, detected at different rates along the evolution of the virus from post onset of the symptoms till convalescence is indicative of viral shedding and can be used to generate the P_c distribution [45]. For influenza, nasal, oral or ocular shedding of H1N1 virus has been detected by determining the relative equivalent unit (REU) from viral RNA level [46]. Such data can be used to generate the P_c distribution (Figure 1.c). Figure 1 shows the viral shedding distributions we generated based on viral shedding for H1N1 influenza and SARS respectively. While we consider maximum infectivity for calculating term incorporates the differences in infectivity due to variations in infectious individuals. The stochasticity in individual's susceptibility is accounted for via the binomial or Poisson distribution.

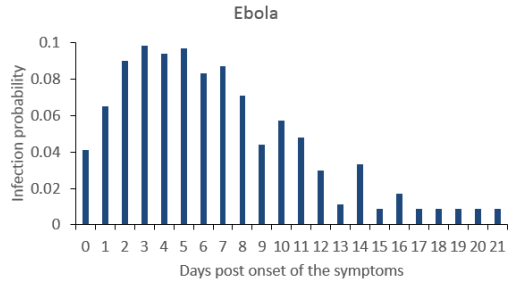

(a)

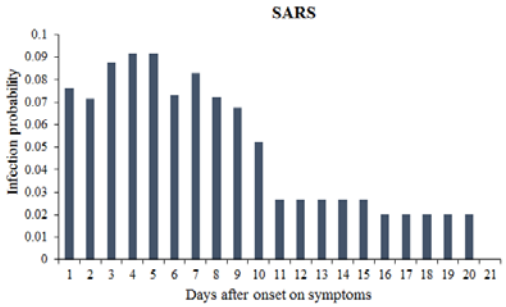

(b)

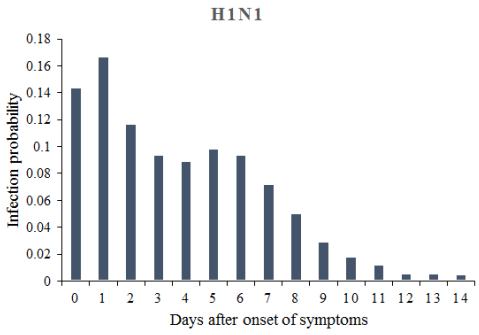

(c)

Figure 1 Infectivity probability distributions (Pc) (a) along the days after clinical signs of Ebola infection, (b) during viral shedding of SARS and (c) H1N1

The distribution of the infective individuals in the crowd is unidentified; any of these pedestrians can be probably infective. We assume that the infectives can be in anywhere among the crowd, so there are many possible permutation patterns of infectives location within the crowd. Denote by "Comb" the possible permutations of infectives which depend on the assumed number of infectives and the total number of the population. All these possible permutations are run successively, and at each run the number of susceptible individuals $S_i(t-1)$ in contact with the

infectives is counted. Then, the number of newly infected individuals is a binomial distribution of the number of individuals in contact $S_i(t-1)$ and probability of success of viral transmission p_i. Repeating the same process for all the infectives with different days of infection c and at different locations in the crowd, further binomial distributions are obtained. Denote by λ the possible number of newly infected pedestrians ranging from zero to the maximum obtained number N_{inf} (λ= 0,…,λ_i,…,N_{inf}). Also let w_i be the frequency of obtaining the same λ_i in the runs. In order to obtain the mean binomial distribution of the number of people infected at time t by all of the infectives with varying age of infection "c", we combine the probability plots and average them as given by:

$$I(t) \sim \sum_{c=1}^{d} \sum_{i=1}^{i_c^0} \{Binomial\ [S_i(t-1), P_m.P_c\ \tfrac{m_i(t-1)}{N}]\}^* w_i\ (\lambda_i) / C \quad (5)$$

Where w_i (λ_i) is the frequency of the mean λ_i repetition during all the possible combinations "C" of infectives. Note that the contacts are defined when pedestrians are within a specific transmission distance which is dependent on the transmission mechanism. Instead of using fixed parameters for defining contact, we will treat contact distance and contact definition as one of the parameters in assessing epidemic spread and vary it over the parameter space to mimic epidemic dispersion in different conditions, within the various pedestrian dynamics configurations associated with winding queues. Based on the above discussion, we vary the contact distance between 2.1 m and 0.9 m which are representative of aerosol and coarse droplet mechanisms respectively. Similarly, the infection probability (P_{inf}) is varied as a parameter up to a value of 0.2 to represent various levels of infectivity.

The Binomial distribution is valid for a large crowd with higher probability of infection. This applies to the winding queues. However, in the situation where N is large and P_{inf} is very small (below 0.1), for instance during boarding and deplaning, the Poisson distribution can be used to approximate the binomial distribution. Here, I(t) is distributed using the Poisson approximation:

$$I(t) \sim \sum_{c=1}^{d} \sum_{i=1}^{i_c^0} \{Poisson\ [S_i(t-1), P_m.P_c\ \tfrac{m_i(t-1)}{N}]\}^* w_i\ (\lambda_i) / C \quad (6)$$

3. RESULTS AND DISCUSSION

We evaluate the role of motion pattern in contact creation between neighboring pedestrians, within a fixed control area, for different stages in air travel including boarding, deplaning and progressing in security check line for different diseases. The passengers, seats and walls are all modelled as particles. We consider the situation of a single infective in the crowd. The infectious individual is unidentifiable; his index in the crowd is not known apriori. Therefore, all permutations of the infectious individual's position are simulated to determine the average number of contacts for a given scenario. We apply these permutations to different aircraft sizes and cabin configurations as well as various security winding queue layouts. We also account different transmission mechanism and probability of pathogens. Airborne viral nuclei vary in size. Expelled fine aerosols travel farther and remain suspended for a longer period of time than coarse droplets. We account for coarse droplets and aerosols transmission mechanisms by varying the contact radius parameter between 0.9 and 2.1 meters (36-84 inches). We vary the transmittance probability between 0.025 and 0.2 to account for the vulnerability and receptivity of the exposed infective to various infection types.

Boarding from a waiting lounge

For boarding, the Airbus A320 carrier with 144 passenger configuration is chosen. During the enplaning, the trajectories of passengers, initially seated or standing in the departure lounge, heading to the passenger boarding bridge and finding their assigned onboard seats, are modelled. The evolution of pedestrian trajectories has been displayed for ingress from a gate in Figure 2. The instantaneous position and speed of each walking individual are obtained by solving equation (1) by means of a predictor-corrector numerical method. Many qualitative features of pedestrian movement are captured by the model. For instance, lane formation is observed in the hallways, in addition to reduced speed at bottlenecks where passengers from different seating zones merge and head to the airplane (Figure 2).

After obtaining the trajectories, the contact data and the number of newly infected travellers are obtained for Ebola and SARS diseases by means of the mathematical epidemiological model. In real life the identity of infectious individual is not known beforehand, therefore all the possible permutations of a single infective are run to estimate the mean of newly infected susceptibles denoted by λ_i where i ranges from 1 to the total passenger capacity of the aircraft. Due to the stochastic nature of the problem, we assume that the number of newly infected travellers by a single infectious chosen randomly among the airplane passengers is Poisson distributed with mean λ_i at every simulation. After performing all the simulations in parallel, the effective probability of means is calculated at peak day of infection. Then, using the Bayes' theorem the probabilities are combined to generate the probability distributions in Figures 3 and 4. These plots represent the probabilistic distribution of infected passengers who were closely exposed to Ebola and SARS viruses.

We consider an infectious passenger at his first day is onboard among the susceptible population. Ebola and H1N1 record a peak of 2 newly infected passengers exposed to the virus, whereas this number increases to 5 for SARS due to the wider range of infectivity. Shifting the infectivity to its highest (day 3 for Ebola, day 5 for H1N1 and day 4 or 5 for SARS), the means of the Poisson distribution increases by one unit for Ebola and SARS but expands tremendously for H1N1 since the infectivity reaches its peak of 30% at the fifth day of H1N1 infection (Figure 4).

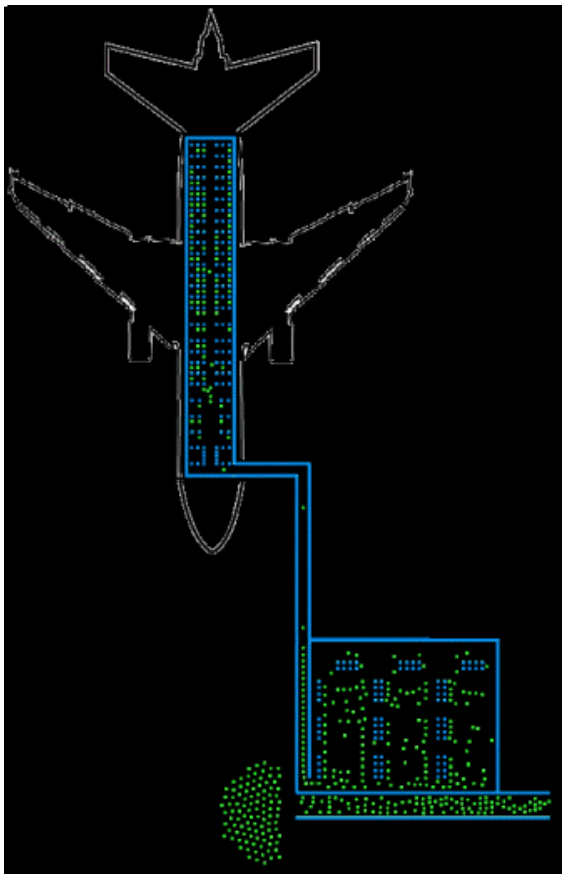

Figure 2. Simulation snapshot of an embarkation of an Airbus A320 from a departure lounge. Green dots represent pedestrian particles and blue dots represent fixed seat and wall particles.

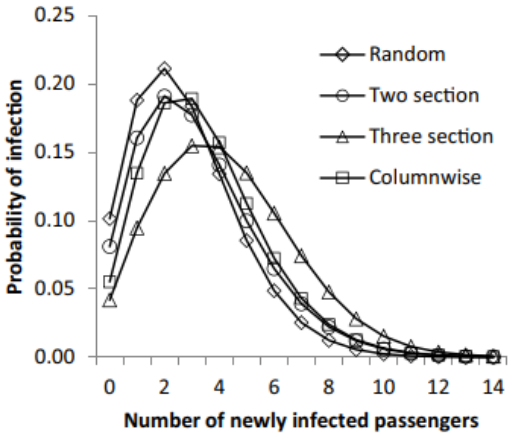

Figure 3. Infection distribution profile for different boarding strategies for an Airbus A320 capable of seating 144 passengers at Ebola peak day of infection (p_{inf} =0.098) and 1.2m contact radius.

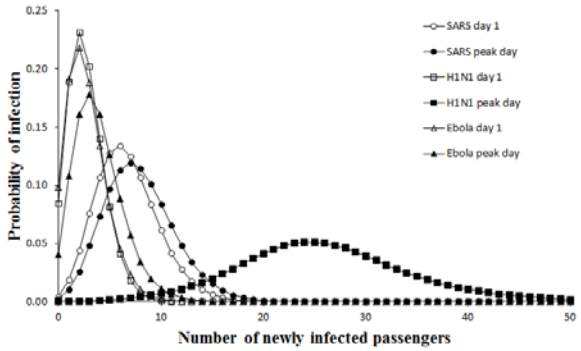

Figure 4. Infection profile at the first and peak days during a random ingress from a lounge to an Airbus A320-144 seats for Ebola, Influenza H1N1 and SARS contagions.

Deplaning from an air carrier

We followed a similar approach for the deplaning strategies and applied it this time for the 182-seat Boeing 757. We found that deplaning had a smaller impact on infection dynamics because of the lower number of new contacts and lower time of exposure during the comparatively faster process. In Figure 5, we show a comparison of different deplaning strategies for the 182-seat Boeing 757 seating configuration for Ebola disease at the peak day of infection. The different deplaning strategies such as alternating columns, alternating rows, zone-wise, and baseline (closest to exit are out first) result in a similar number of mean infective individuals. When we compare the probabilities, alternate rows and baseline strategies are marginally better.

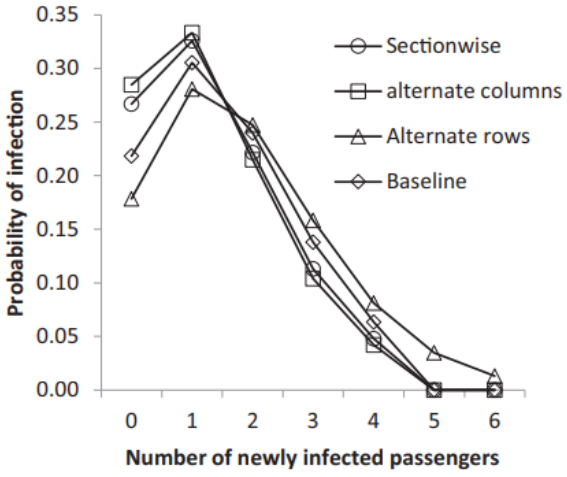

Figure 5. Infection distribution profile for different deplaning strategies for a 182-seat Boeing 757 at Ebola peak day of infection (p_{inf} =0.098) and 1.2m contact radius.

The effect of size of airplane on the number of contacts and thereby infection spread is assessed. We model the seating arrangements for five different airplanes. The seating arrangement is as shown in Figure 6. Figure 7 shows the number of contacts for transporting 1000 passengers using the different airplane models considered. These numbers include default boarding and deplaning methods on multiple flights with a particular airplane model to

transport 1000 passengers. Smaller airplanes are more effective in reducing the number of contacts compared to larger airplanes; however, the advantage of airplane size reduces as airplane seating capacity increases.

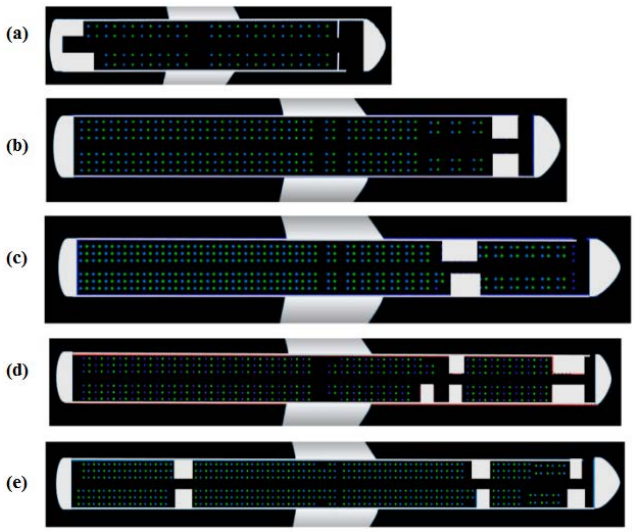

Figure 6. Airplane configurations considered in the study (a) CRJ200 with 50 seats, (b) A320 with 144 seats (c) Boeing 757-200 with 182 seats, (d) Boeing 757-200 with 201 seats and (e) Boeing 757-300 with 240 seats. Green dots represent pedestrian particles and blue dots represent fixed seat particles.

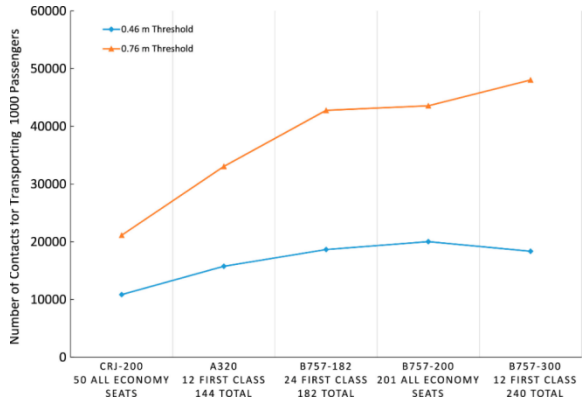

Figure 7. Number of contacts for transporting 1000 passengers in different airplanes boarding and deplaning by default methods.

Infectious Disease Spread in an Airport Security Queue

Reports indicate that travellers are delayed for more than an hour at screening checkpoints, causing significant economic burden on airlines [48]. Screening procedure at checkpoints only involves the passengers and their carry-on baggage. However, no equipment is available for use to detect viral contagions during an outbreak. Consequently, security checkpoints with people congregated in winding queues are a potential hotspot for infectious disease spread.

In investigating the relation between the layout shape and the contact among pedestrians in queues, we simulate different security line winding queues by changing the aisles and zones layout based on actually observed queue configurations in airports (Figure 8). With time evolution, the pedestrians move forward in the sequence to reach the exit. It is expected that the aisle's length, direction and structure within the control area, and the distribution of turn corners have an effect on the contact between pedestrians.

We consider the case of pedestrians arranging in a rectangular queue. At initial conditions, the pedestrians are distributed in abreast (side-by-side) manner in the aisles. The formation of groups (family members, group of tourists, etc.) is taken into consideration by the close abreast queues whereas individual travellers tend to form a more spaced single line as mentioned in the formulation section (Figure 8.b).

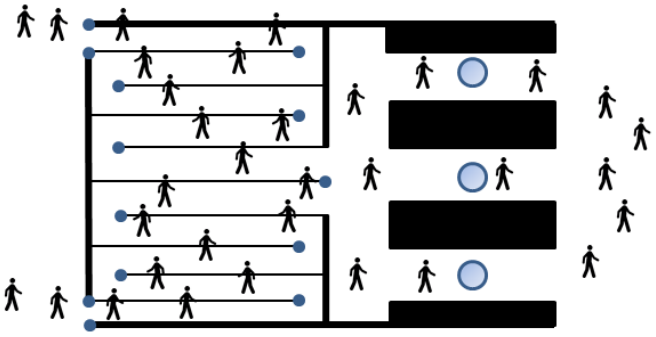

(a)

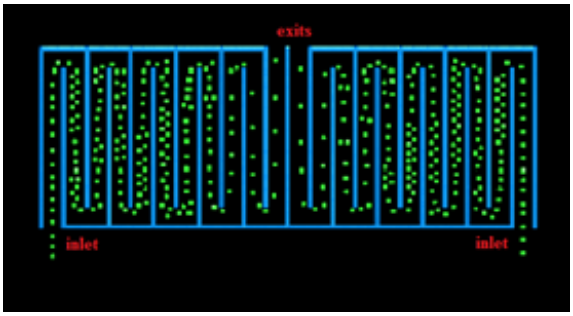

(b)

Figure 8. Security check floor map (a) in an airport, (b) from simulation.

Four different rectangular queue configurations of the same area, as shown in Figure 9, are analyzed. The four rectangular floor plans are either split vertically (configurations (b) and (c)) or horizontally (configurations (a) and (d)). Configurations (a) and (b) have one inlet and one exit whereas configurations (c) and (d) have two inlets and two exits due to the existence of separated zones. The width of the pedestrian lanes remains 1 meter, which allows some pedestrians belonging to the same group to form a double line.

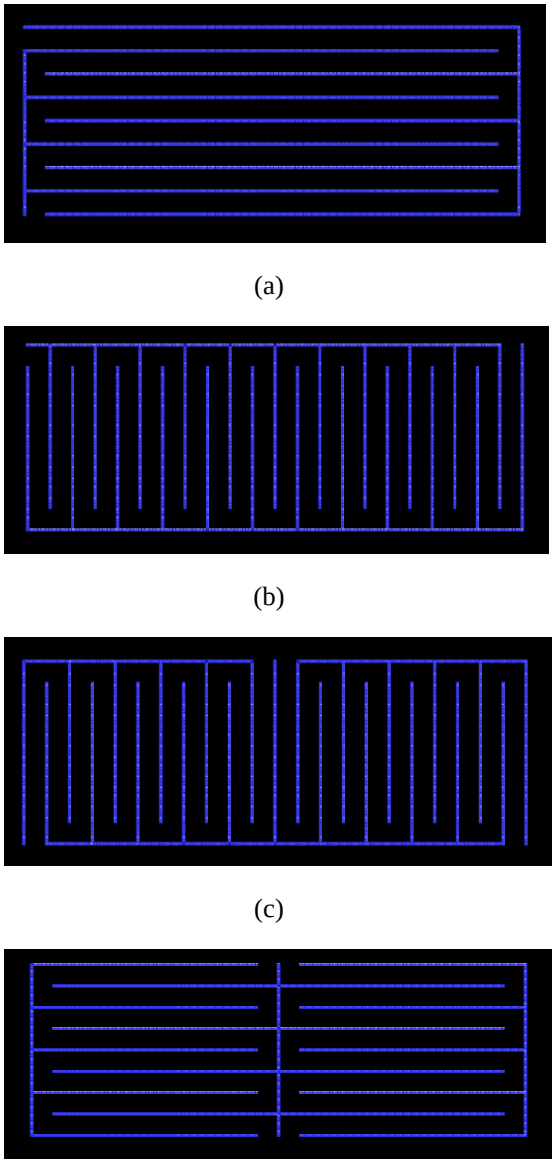

Figure 9. Rectangular winding queue layouts: (a) Config.1, (b) Config.2, (c) Config.3, (d) Config.4.

Instead of limiting the analysis to certain disease type or mechanism, we generalize the study by sweeping the infection parameters (infection probability and contact radius) over their ranges of definition. We vary the contact distance between 2.1 m and 0.9 m which are representative of aerosol and coarse droplet mechanisms respectively. Similarly, the infection probability (P_{inf}) is varied as a parameter up to a value of 0.2 to represent various levels of infectivity.

The mean number of newly infected pedestrians is then obtained by combining the number of contacts within a given contact radius, with the infection transmission probability described earlier. The mean number of newly infected is binomially distributed to account for the demographic stochasticity in the immunity and receptivity of the susceptible population. Under different infection scenarios, the mean number of newly infected exposed individuals is obtained. In the following, only the peak dispersion of the disease (the mean of the binomial distribution) among the susceptible population is plotted over the parameters space of variation.

With the commonly used rope separators and at a proximate, direct contact via coarse droplets (radius of infection less than 1.2m), the infective has influence on only the directly adjacent aisles on both sides. However, infection also relies on the transmission probability. In other words, not every contact will lead to infection. For a defenceless (unimmunized) individual, the probability to contract the disease alters between 2.5 and 20% depending on the disease development time and its survival in the ambient environment. Combining the contact data with the infection model leads to the mean distribution of infection over the probability range. Configurations 3 is the best layout for all transmission probabilities, followed by configuration 2 (Figure 10). In configuration 2, the vertical aisles are short, which means less capacity of pedestrians. Configuration 3 has the same aisle geometry as of configuration 2. However, the pedestrian will exit the queue earlier (half way) compared to that of configuration 2 which results in lower exposure time. Configurations 1 and 4 result in a higher mean number of infections. These configurations have long open aisles compared to configurations 2 and 3 with the lower aisle length. Therefore, more pedestrians are involved and interaction occurs more frequently with pedestrians from neighbouring aisles in these two configurations. Configuration 1 is the least favourable layout because diverse pedestrians from both sides come into proximity more frequently than in configuration 4 with comparatively shorter aisles. Configuration 4 is worse than configuration 2 because at the common corners between the left and right zones, the infective comes into contact with additional pedestrians from the neighbouring zones.

Figure 10 also shows the results of repeating the transmission probability variation over the same range, but assuming aerosol transmission mechanism with a longer contact radius of 2.1 m. Configuration 3 still results in the lowest number of contacts for both rope and wall separators. For rope separator, we observe the same pattern of results as with the coarse droplets transmission mechanism, but with increased infection spread. The similarity between the configurations increases especially at low transmission probabilities. Therefore, the results of configurations 2 and 3, as well as configurations 1 and 4 overlap. At 2.1 m radius, the dispersion of the fine viral particles crosses the aisle boundaries to two adjacent aisles on each side. Here, the findings of configurations 2 and 3 are nearly identical since the aisles are distributed in the same manner except that configuration 3 has two separated zones. When the transmission radius expands to many neighbouring aisles, pedestrians of one zone in configuration 3 come into contact not only with other pedestrians within the same zone, but to others in the adjacent zone. Accordingly, configurations 2 and 3 have the same behavior. Here, the separation of these two groups has no effective role in reducing contact. The same principle applies to configurations 1 and 4; the offset between the data of configurations 1 and 4 is reduced compared to that of coarse droplet transmission mechanism

for the same reason. Configuration 1 remains the worst layout, especially at higher probabilities, due to the elongated, abundant contact between pedestrians from adjacent aisles.

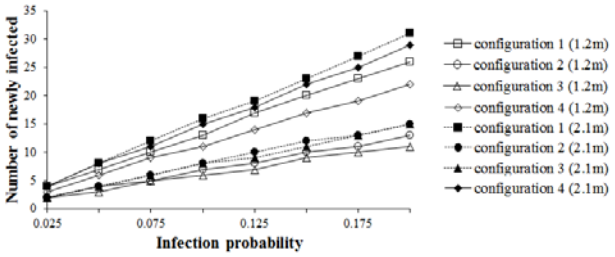

Figure 10. Infection distribution profile for different abreast queue configurations at contact radii of 1.2m (coarse droplets) and 2.1m (fine aerosols).

We now explore the contacts generated between pedestrians in the four configurations assuming different infection mechanisms represented by the radius variation. We suggest placing temporary walls between the aisles to suppress the propagation of the outbreak among the waiting crowd. For rope separators previously evaluated, contact extends to pedestrians in the neighbouring aisles, whereas for temporary walls, transmission due to contact is limited only between the pedestrians within the same aisle.

Configurations 2 and 3 result in lower number of infections for rope separators, across the range of infection radii from 0.9 to 2.1 m as shown in Figure J. As explained, for aisles separated with ropes, shorter aisles lead to lower exposure of an infective resulting in this behavior. For walls, the combination of the radius of infection, as well as the interaction time within the aisles and at the corners alter the results (Figure 11). Each combination of contact radius and queue layout generates a different number of newly infected individuals. At low radii, short-aisle and low exit time configurations are favourable. At higher radii, configurations with less turning corners are better. The wall separator has drastically reduced the number of infections compared to the conventionally used rope stanchions.

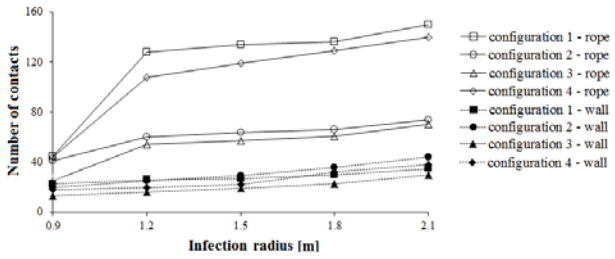

Figure 11. Contact distribution for different abreast queue configurations. The contact radius is varied for both wall and rope aisle separation scenarios.

4. CONCLUSIONS

A multiscale model combining social-force-based pedestrian dynamics and the individual based stochastic infection dynamics model has been formulated. The model is used to study the dynamics of infectious disease spread in airplanes and airports. Specific air-travel-related policies that potentially mitigate diseases spread are identified. A two-section boarding has an effect on reducing disease propagation aboard an airplane. Deplaning has no effect and all deplaning strategies generated a single infected traveller. Small airplanes are more effective in reducing the number of contacts during an outbreak. We find that the layout of winding queues in airport security check influences the number of new infections. The modeling approach developed here is generic and can be readily modified to other directly transmitted infectious diseases and dense pedestrian spaces.

5. ACKNOWLEDGMENT

This research was partially supported by NSF ACI and DOT UTC Center for Advanced Transportation Mobility.

REFERENCES

1. M. E. Wilson, “Travel and the emergence of infectious diseases,” Emerging infectious diseases, vol. 1, no. 2, p. 39, 1995.
2. Center for Disease Control (CDC), “Interstate importation of measles following transmission in an airport--California, Washington, 1982.,” MMWR. Morbidity and mortality weekly report, vol. 32, no. 16, pp. 210, 215, 1983.
3. M. R. Moser, T. R. Bender, H. S. Margolis, G. R. Noble, A. P. Kendal, and D. G. Ritter, “An outbreak of influenza aboard a commercial airliner,” American journal of epidemiology, vol. 110, no. 1, pp. 1–6, 1979.
4. S. J. Olsen et al., “Transmission of the severe acute respiratory syndrome on aircraft,” New England Journal of Medicine, vol. 349, no. 25, pp. 2416–2422, 2003.
5. M. J. Tracy, “Transmission of tuberculosis during a long airplane flight.,” The New England journal of medicine, vol. 335, no. 9, pp. 675; author reply 675-6, 1996.
6. M.-A. Widdowson et al., “Probable transmission of norovirus on an airplane,” Jama, vol. 293, no. 15, pp. 1855–1860, 2005.
7. Mangili and M. A. Gendreau, “Transmission of infectious diseases during commercial air travel,” The Lancet, vol. 365, no. 9463, pp. 989–996, 2005.
8. M. G. Baker et al., “Transmission of pandemic A/H1N1 2009 influenza on passenger aircraft: retrospective cohort study,” Bmj, vol. 340, p. c2424, 2010.
9. S. Namilae, P. Derjany, A. Mubayi, M. Scotch, and A. Srinivasan, “Multiscale model for pedestrian and infection dynamics during air travel,” Physical review E, vol. 95, no. 5, p. 052320, 2017.
10. S. Namilae, A. Srinivasan, A. Mubayi, M. Scotch, and R. Pahle, “Self-propelled pedestrian dynamics model: Application to passenger movement and infection propagation in airplanes,” Physica A: Statistical Mechanics and its Applications, vol. 465, pp. 248–260, 2017.

11. Srinivasan, C. D. Sudheer, and S. Namilae, “Optimizing massively parallel simulations of infection spread through air-travel for policy analysis,” in 2016 16th IEEE/ACM International Symposium on Cluster, Cloud and Grid Computing (CCGrid), 2016, pp. 136–145.
12. P. Derjany and S. Namilae, “Computational Model for Pedestrian Movement and Infectious Diseases Spread During Air Travel,” in 2018 AIAA Modeling and Simulation Technologies Conference, 2018, p. 0419.
13. S. Chunduri, M. Ghaffari, M. S. Lahijani, A. Srinivasan, and S. Namilae, “Parallel low discrepancy parameter sweep for public health policy,” in 2018 18th IEEE/ACM International Symposium on Cluster, Cloud and Grid Computing (CCGRID), 2018, pp. 291–300.
14. C. Burstedde, K. Klauck, A. Schadschneider, and J. Zittartz, “Simulation of pedestrian dynamics using a two-dimensional cellular automaton,” Physica A: Statistical Mechanics and its Applications, vol. 295, no. 3–4, pp. 507–525, 2001.
15. L. F. Henderson, “The statistics of crowd fluids,” nature, vol. 229, no. 5284, pp. 381–383, 1971.
16. S. Okazaki and S. Matsushita, “A study of simulation model for pedestrian movement with evacuation and queuing,” in International Conference on Engineering for Crowd Safety, 1993, vol. 271.
17. D. Helbing and P. Molnar, “Social force model for pedestrian dynamics,” Physical review E, vol. 51, no. 5, p. 4282, 1995.
18. D. Helbing, I. Farkas, and T. Vicsek, “Simulating dynamical features of escape panic,” Nature, vol. 407, no. 6803, p. 487, 2000.
19. M. Treiber, A. Hennecke, and D. Helbing, “Derivation, properties, and simulation of a gas-kinetic-based, nonlocal traffic model,” Physical Review E, vol. 59, no. 1, p. 239, 1999.
20. S. Wei-Guo, Y. Yan-Fei, W. Bing-Hong, and F. Wei-Cheng, “Evacuation behaviors at exit in CA model with force essentials: A comparison with social force model,” Physica A: Statistical Mechanics and its Applications, vol. 371, no. 2, pp. 658–666, 2006.
21. F. Li, S. Chen, X. Wang, and F. Feng, “Pedestrian evacuation modeling and simulation on metro platforms considering panic impacts,” Procedia-social and behavioral sciences, vol. 138, pp. 314–322, 2014.
22. R. Mehran, A. Oyama, and M. Shah, “Abnormal crowd behavior detection using social force model,” in 2009 IEEE Conference on Computer Vision and Pattern Recognition, 2009, pp. 935–942.
23. F. Zanlungo, T. Ikeda, and T. Kanda, “Social force model with explicit collision prediction,” EPL (Europhysics Letters), vol. 93, no. 6, p. 68005, 2011.
24. G. Lämmel and M. Plaue, “Getting out of the way: Collision-avoiding pedestrian models compared to the realworld,” in Pedestrian and Evacuation Dynamics 2012, Springer, 2014, pp. 1275–1289.
25. M. Schultz, S. Lehmann, and H. Fricke, “Pedestrian dynamics in airport terminals considering emergency cases,” Proceedings of Internation Council of the Aeronautical Sciences, 2006.
26. W. Ma., “Agent-based model of passenger flows in airport terminals,” Doctoral dissertation, Queensland University of Technology. 2013
27. L. Cheng,, “Modelling airport passenger group dynamics using an agent-based method,” Doctoral dissertation, Queensland University of Technology. 2014
28. Y.-H. Lin and C.-F. Chen, “Passengers’ shopping motivations and commercial activities at airports–The moderating effects of time pressure and impulse buying tendency,” Tourism Management, vol. 36, pp. 426–434, 2013.
29. B. Kraal, V. Popovic, and P. J. Kirk, “Passengers in the airport: artefacts and activities,” in Proceedings of the 21st Annual Conference of the Australian Computer-Human Interaction Special Interest Group: Design: Open 24/7, 2009, pp. 349–352.
30. V. Popovic, B. Kraal, and P. J. Kirk, “Towards airport passenger experience models,” in Proceedings of 7th international conference on design & emotion, 2010.
31. S. Kalakou, F. Moura, and V. Medeiros, “Analysis of airport configuration and passenger behaviour,” in Proceedings of the 10th International Space Syntax Symposium, 2015.
32. J. Zębala, P. Ciępka, and A. RezA, “Pedestrian acceleration and speeds,” Problems of Forensic Sciences, vol. 91, pp. 227–234, 2012.
33. M. Moussaïd, N. Perozo, S. Garnier, D. Helbing, and G. Theraulaz, “The walking behaviour of pedestrian social groups and its impact on crowd dynamics,” PloS one, vol. 5, no. 4, p. e10047, 2010.
34. M. T. Osterholm et al., “Transmission of Ebola viruses: what we know and what we do not know,” MBio, vol. 6, no. 2, pp. e00137-15, 2015.
35. S. Judson, J. Prescott, and V. Munster, “Understanding ebola virus transmission,” Viruses, vol. 7, no. 2, pp. 511–521, 2015.
36. M. Nikiforuk, T. A. Cutts, S. S. Theriault, and B. W. Cook, “Challenge of liquid stressed protective materials and environmental persistence of ebola virus,” Scientific reports, vol. 7, no. 1, p. 4388, 2017.
37. R. P. Clark and M. L. de Calcina-Goff, “Some aspects of the airborne transmission of infection,” Journal of the Royal Society Interface, vol. 6, no. suppl_6, pp. S767–S782, 2009.
38. R. W. K. Li, K. W. C. Leung, F. C. S. Sun, and L. P. Samaranayake, “Severe Acute Respiratory Syndrome (SARS) and the GDP. Part I: Epidemiology, virology, pathology and general health issues,” British dental journal, vol. 197, no. 2, p. 77, 2004.

39. K. Y. Yuen and S. S. Y. Wong, “Human infection by avian influenza A H5N1,” Hong Kong Medical Journal, 2005.
40. L. Bourouiba, E. Dehandschoewercker, and J. W. Bush, “Violent expiratory events: on coughing and sneezing,” Journal of Fluid Mechanics, vol. 745, pp. 537–563, 2014.
41. J. K. Gupta, C.-H. Lin, and Q. Chen, “Flow dynamics and characterization of a cough,” Indoor air, vol. 19, no. 6, pp. 517–525, 2009.
42. H. M. Friesema et al., “Norovirus outbreaks in nursing homes: the evaluation of infection control measures,” Epidemiology & Infection, vol. 137, no. 12, pp. 1722–1733, 2009.
43. N. Jaax et al., “Transmission of Ebola virus (Zaire strain) to uninfected control monkeys in a biocontainment laboratory,” The Lancet, vol. 346, no. 8991–8992, pp. 1669–1671, 1995.
44. S. Towner et al., “Rapid diagnosis of Ebola hemorrhagic fever by reverse transcription-PCR in an outbreak setting and assessment of patient viral load as a predictor of outcome,” Journal of virology, vol. 78, no. 8, pp. 4330–4341, 2004.
45. G. Zhao, “SARS molecular epidemiology: a Chinese fairy tale of controlling an emerging zoonotic disease in the genomics era,” Philosophical Transactions of the Royal Society B: Biological Sciences, vol. 362, no. 1482, pp. 1063–1081, 2007.
46. S. G. Paquette et al., “Influenza transmission in the mother-infant dyad leads to severe disease, mammary gland infection, and pathogenesis by regulating host responses,” PLoS pathogens, vol. 11, no. 10, p. e1005173, 2015.
47. G. Bender., “Airport Terminal Security Screening Checkpoints: Still An Industrial Engineering Problem,” Retrieved from https://www.arenasimulation.com/blog/post/airport-terminal-security-screening-checkpoints-still-an-industrial-engineer, 2016**.**

Biography

Pierrot Derjany *is about to complete his PhD in Aerospace Engineering at Embry-Riddle Aeronautical University. He works on combining the principles of molecular dynamics, pedestrian movement and epidemic modelling to study infectious disease spread during air travel.*

Dr. Sirish Namilae *is an Associate Professor in Aerospace Engineering at Embry-Riddle Aeronautical University with substantial industrial experience at the Department of Energy and at Boeing Rotorcraft. His research expertise is in the areas multiscale modeling, particle dynamics and composite materials.*

Dr. Dahai Liu *is a Professor in the School of Graduate studies at the college of Aviation, Embry-Riddle Aeronautical University. His research interests lie in the area of systems engineering, human computer interaction, and human factors in aerospace and aviation.*

Dr. Ashok Srinivasan *is the William Nystul Eminent Scholar Chair and Professor of Computer Science at the University of West Florida. His research expertise lies in high-performance computing, with a focus on applications of supercomputing to science and public policy*